Engineering Geology 341 (2024) 107690

Contents lists available at ScienceDirect

Engineering Geology

journal homepage: www.elsevier.com/locate/enggeo

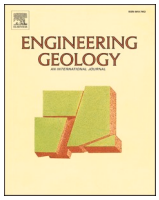

Near-surface soil hydrothermal response feedbacks landslide activity and mechanism

Xiao Ye [a,b], Hong-Hu Zhu [a,*], Bing Wu [a], Feng Tian [a], Wei Zhang [a,*], Xie Hu [c], Luca Schenato [d], Alessandro Pasuto [e], Filippo Catani [b]

[a] School of Earth Sciences and Engineering, Nanjing University, Nanjing 210023, China
[b] Department of Geosciences, University of Padova, Padova 35131, Italy
[c] College of Urban and Environmental Sciences, Peking University, Beijing 100871, China
[d] Department of Information Engineering, University of Padova, Padova 35131, Italy
[e] National Research Council-Research Institute for Geo-Hydrological Protection (CNR-IRPI), Padova 35127, Italy

ARTICLE INFO

Keywords:
Slow-moving landslide
Geo-interface
Ground temperature
Soil moisture content
Extreme weather event

ABSTRACT

Surface moisture has recently been reported to be used in regional-scale landslide early warning. Nevertheless, near-surface multi-depth hydrothermal measurements as a hillslope scale are often less concerned and rarely linked to landslide kinematics. In this paper, we selected two neighboring landslides with different deformation mechanisms as case studies. Using in-situ multi-source sensors, we monitored real-time soil temperature and moisture at specific depths within approximately 1.5 m. The measurements span two complete monsoon seasons, representing concurrent dry and wet hydrological extremes. Statistical Pearson correlation analysis was employed to quantify the relationships between landslide activity and environmental variables such as soil temperature and moisture content. The results indicate that the near-surface soil temperatures and moisture contents contribute to a better understanding of the factors controlling landslide activity, in which variations synergistically reflect hydrothermal interaction and potential deformation mechanisms. These soil temperatures and moisture contents at certain depths (specifically at 20, 50, and even 100 cm) show moderate to strong correlations (with Pearson correlation coefficient values ranging from 0.4 to 0.8) with landslide deformation. In cases where discrete daily rainfall data exhibited unsatisfactory correlations due to their data attributes, soil temperature and moisture effectively served as alternative indicators for rainfall inputs, aiding in the analysis. Overall, this work emphasizes the critical influence of soil moisture and temperature on landslide dynamics. This study also highlights the need for comprehensive monitoring and forecasting strategies that consider a wide range of environmental factors to mitigate landslide risks associated with climate change, particularly in the context of intensified extreme weather events.

1. Introduction

Active slow-moving landslides and rockslides are general natural hazards on our planet (Froude and Petley, 2018; Fang et al., 2024; Ye et al., 2024a). In addition to the instant hazards caused by landslide failures, potential geo-risks that slow-moving landslides pose to infrastructure and human habitats are of more concern (Lacroix et al., 2020; Shi et al., 2021; Zeng et al., 2023; Xie et al., 2024; Ye et al., 2024b). The warming climate is currently reshaping the balance between natural and human systems, potentially pushing these risks to more challenging levels (Kirschbaum et al., 2020; Araújo et al., 2022; Stevenson et al., 2022). To mitigate this situation, scientific observations and in-depth interpretations of monitoring data play a crucial role (Hu et al., 2020; Pei et al., 2023; Zeng et al., 2024b). It is widely recognized that multi-source, multi-physical monitoring tends to unveil the real state and evolutionary processes of landslides (Seguí and Veveakis, 2021; Ye et al., 2022, 2024c), especially the interaction mechanism of critical underground geo-interfaces (Zhu, 2023). However, near-surface thermo- and

* Corresponding authors.
E-mail addresses: yexiao@smail.nju.edu.cn (X. Ye), zhh@nju.edu.cn (H.-H. Zhu), wb@smail.nju.edu.cn (B. Wu), tianfeng@smail.nju.edu.cn (F. Tian), wzhang@nju.edu.cn (W. Zhang), hu.xie@pku.edu.cn (X. Hu), luca.schenato@unipd.it (L. Schenato), alessandro.pasuto@irpi.cnr.it (A. Pasuto), filippo.catani@unipd.it (F. Catani).

https://doi.org/10.1016/j.enggeo.2024.107690
Received 11 April 2024; Received in revised form 8 July 2024; Accepted 19 August 2024
Available online 22 August 2024

hydro-related measurements have received less attention and are rarely linked to slope stability, except in cold regions involving permafrost dynamics (Patton et al., 2021; Wu et al., 2021; Zhu et al., 2023).

Traditionally, ground temperature is not the primary target in landslide monitoring. The effect of temperature on landslide stability usually involves thermally induced increases in pore water pressure associated with frictional heat dissipation to explain the catastrophic acceleration of large landslides (Voight and Faust, 1982; Veveakis et al., 2007; Goren and Aharonov, 2007, 2009; Pinyol and Alonso, 2010; He et al., 2015; Alonso et al., 2016; Pinyol et al., 2018). Surface temperature changes are generally not considered to be a direct driver of landslide destabilization (Loche et al., 2022; Loche and Scaringi, 2023; Fang et al., 2023). Instead, precipitation and reservoir-induced groundwater level variations are recognized as primary triggers of landslides (Yin et al., 2016; Zeng et al., 2022; Zhou et al., 2022; Nava et al., 2023; Liu et al., 2024). More importantly, these landslide drivers may involve spatio-temporal variability (Chang et al., 2023; Ma and Mei, 2024; Ye et al., 2024b). Changes in shallow soil water content can significantly influence feedback from precipitation and snowmelt events (Martelloni et al., 2013; Ahmad et al., 2024; Wistuba et al., 2024), providing insights into landslide hydro-geomechanics. As illustrated in Fig. 1, soil moisture content plays a crucial role in the exchange of water, energy, and carbon between the land and the atmosphere (Ng et al., 2022). Over daily, quarterly, and even yearly timescales, the changes in soil moisture and temperature at the surface may exhibit some complex nonlinear relationships due to rainwater infiltration and evapotranspiration (Eltahir, 1998; Guo et al., 2023b; Wu et al., 2023). This implies that variations in surface soil temperature and moisture content may be linked to landslide deformation and could, in turn, predict landslide stability (Loche and Scaringi, 2024). One of the most notable cases might be the Touge landslide, indicating that seasonal decreases in ground temperature can trigger shallow landslides (Shibasaki et al., 2016). However, due to the scarcity of case reports, understanding of how changes in land temperature and moisture contribute to landslide activity remains limited.

Remote sensing can provide long-term, spatially explicit information on surface temperature and humidity at a low cost, and is particularly useful in mountainous areas with challenging topography (Han et al., 2023; Ye et al., 2024a). This undoubtedly holds significant value for the assessment of landslide susceptibility and early warning on a regional scale (Shi et al., 2021; Zeng et al., 2024a). However, this technique may not necessarily generalize to single landslides that face significant risks of destabilization. This is because once the distance between soil moisture stations and landslides are too large to yield any local predictive value (Wicki et al., 2020). To correctly assess the effects of soil temperature and moisture on landslide activity, therefore, it probably has to rely on precise in-situ instrumentation. More importantly, such measurements allow us to understand soil temperature and moisture characteristics at different depths, unveiling the shallow soil-atmosphere interaction (Sun et al., 2022; Zhu et al., 2024). Currently, methods for measuring and estimating soil temperature and moisture content mainly involve neutron scattering, capacitance- or resistance-based humidity sensors, frequency domain reflectometry (FDR), time domain

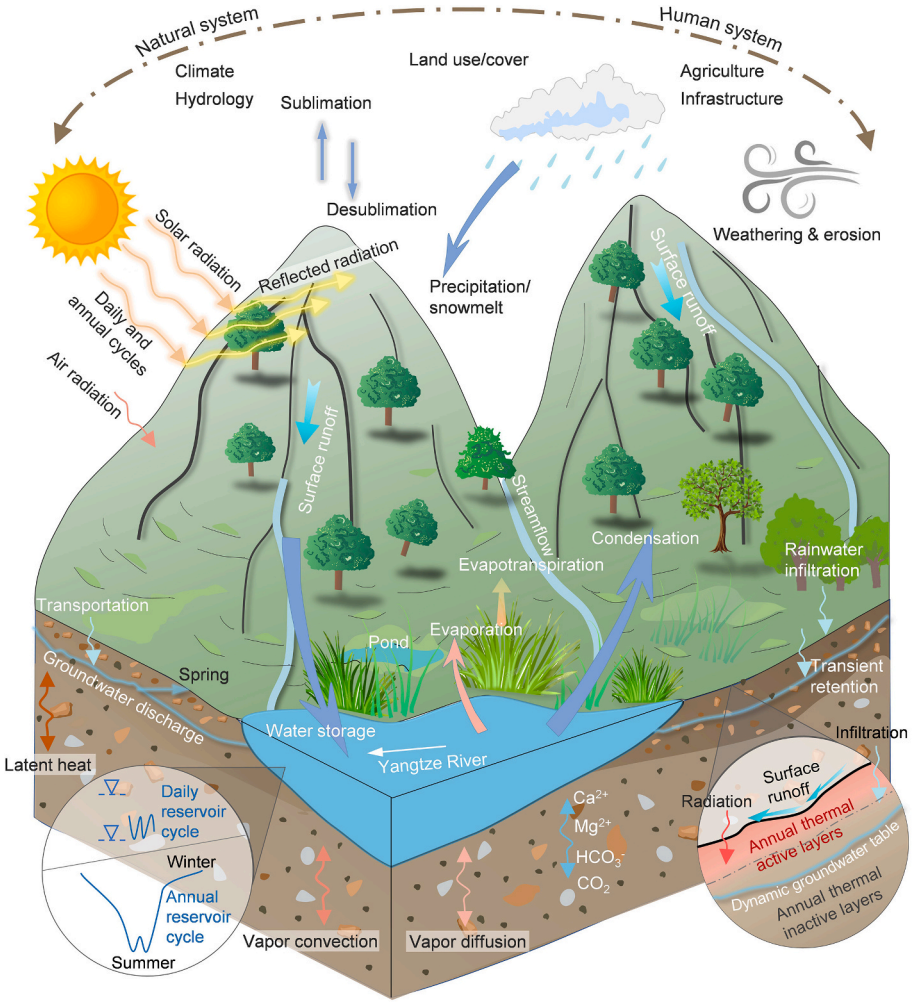

Fig. 1. Illustration of different boundary conditions affecting river bank slopes, and thermo-hydro-chemo-mechanical cycles involved in a natural and human environment.

reflectometry (TDR), and actively heated fiber optic (AH-FO) techniques (Sun et al., 2021; Guo et al., 2024; Wang et al., 2024). The selection of a specific method often depends on its suitability for the intended application scenario and monitoring requirements, with its applicability to landslide assessment rarely considered.

The motivation for this study arises from the urgent need to understand how near-surface soil conditions, which are readily affected by climatic extremes, influence landslide behavior. To investigate the correlation between hillslope-scale landslide activity and near-surface temperature and moisture, real-time, depth-specific soil temperature and moisture data deepened to approximately 1.5 m were obtained through in-situ multi-source sensors including FDR, TDR, fiber optic (FO) sensors, and RC-4. We selected two active neighboring landslides that are driven by distinct mechanisms, to ensure that landslide activity could be appropriately characterized (Zhou et al., 2022, 2024). These measurements temporally cover the past 2 years of 2022 and 2023, and represent two concurrent dry and wet hydrologic extremes. This climatic setting provides a perfect opportunity to investigate the influence of shallow soil temperatures and moisture contents on landslide activity. The target variables reflecting landslide activity include surface displacements (i.e., along a typical profile of each landslide), strains at the surface soil, the slip zone, or the base-cover interface. Statistical Pearson correlation analysis was used to describe the relationships between these target deformation variables and surficial temperature and moisture.

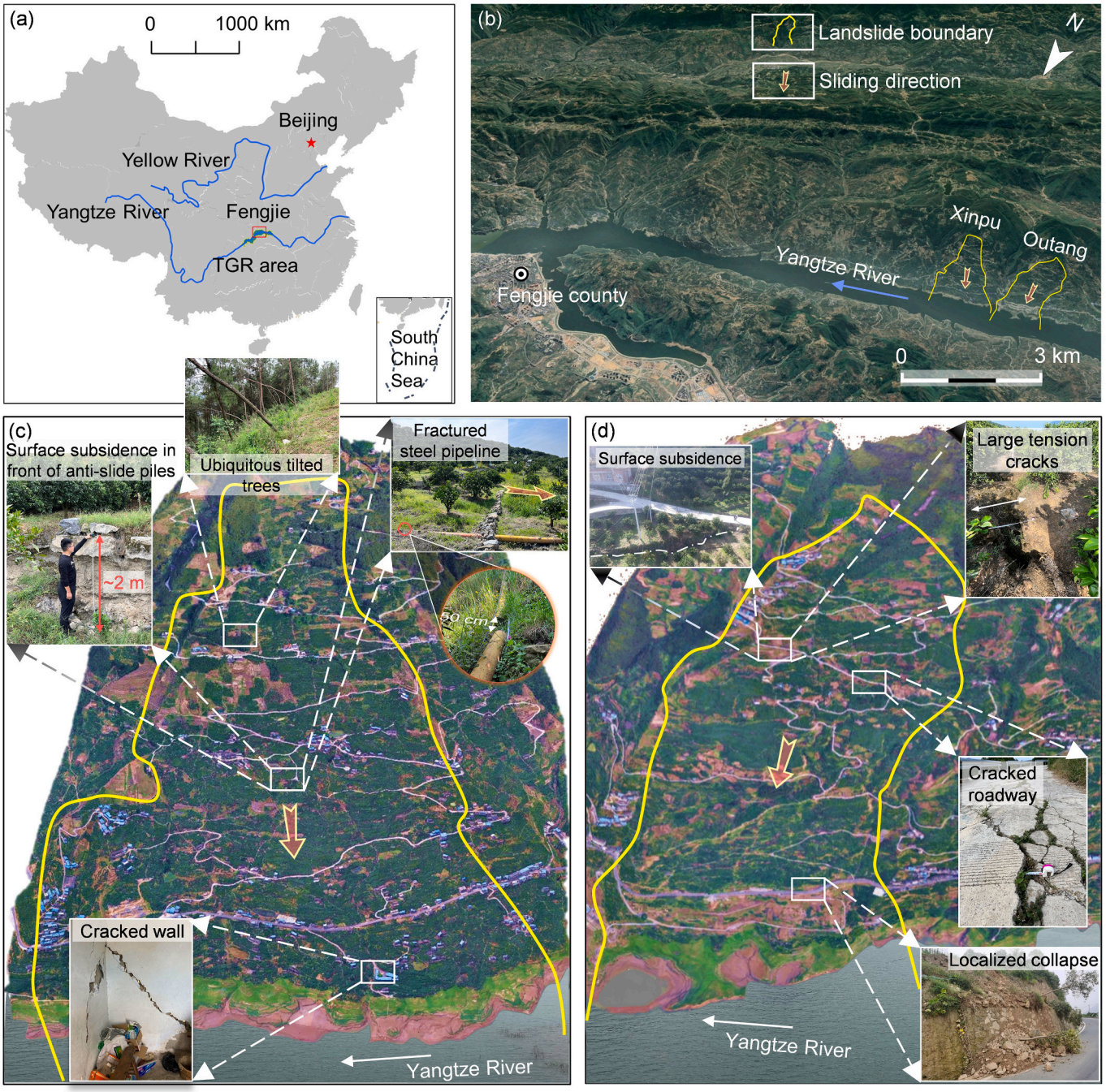

Fig. 2. Geographical and geomorphological setting of the study area. (a) Map of China. (b) Location of the investigated case superimposed on the Google Earth optical image (taken in April 2018, when the RWL was 162.27 m.a.s.l.). (c) and (d) Aerial photographs (taken on 31 May 2021) of the Xinpu landslide and Outang landslide, respectively, as well as representative macroscopic deformation.

Furthermore, by extending the hydrological triggers of landslides into the broader domain of temperature effects on slope stability, this study aims to bridge the gap between near-surface hydrothermal measurements and landslide activity even mechanism, particularly in the context of enhanced extreme weather events.

2. Data and methods

2.1. Study area

The study area is located in Fengjie County, one of the most severely geohazardous areas in the Three Gorges Reservoir (TGR) region, China.

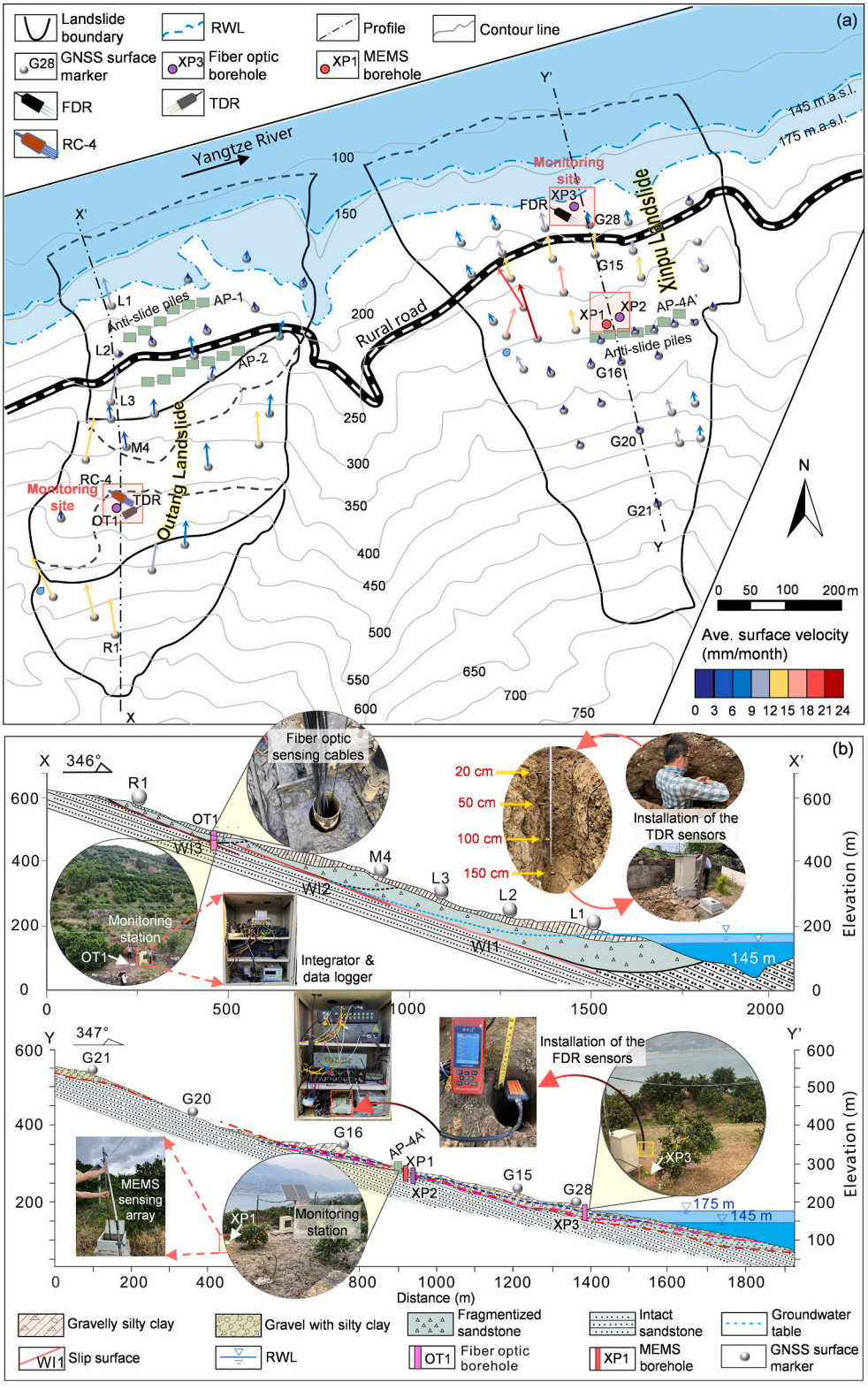

Fig. 3. Plan and profile map of the investigated landslides. (a) Field instrumentation and historical surface velocity vectors in the past decade. (b) Typical profile of the landslides and field installation.

Given their immensely hazardous impacts, we selected two extremely large-scale landslide cases but with different mechanisms, the Outang landslide and the Xinpu landslide, which are spatially separated by a large gully, 2 km apart, for field observations (Figs. 2 and 3). The landslide areas are absent of active faults. Generally, lithology is the core factor controlling the distribution of landslide disasters in the TGR area, while fluctuations in reservoir water level (RWL) and rainfall have historically been considered the main triggering factors for these landslides (Yin et al., 2016; Tang et al., 2019). Rainfall is usually concentrated in the summer, with an annual precipitation of around 1000 mm. Since the impoundment to 175 m.a.s.l. in October 2010, the RWL has fluctuated within the range of 145–175 m.a.s.l. throughout the year.

2.1.1. Outang landslide

The Outang landslide is located on the right bank of the Yangtze River, covering a total area of 1.77 km^2 and a volume of more than 9.0 × 10^7 m^3, making it one of the largest ancient landslides in the TGR area. As early as 2006 or even earlier, the safety of the landslide attracted widespread attention. By October 2010, over 160 cracks were observed, with evident deformation signals throughout the entire landslide (Yin et al., 2016). Monitoring data indicated that landslide displacements mainly occurred during the period from May to September of each year when the RWL normally decreased, whereas displacements were significantly less during the period of filling of RWL or almost the highest RWLs from October to March of the following year.

The elevations of the landslide toe and crown are approximately 90 and 705 m.a.s.l., respectively, with the toe extending into the Yangtze River; the average slope is almost 25°. The slip zone, with a thickness of 0.1–3.2 m, mainly consists of gray-black carbonaceous shale interbedded with mudstone. The bedrock orientation ranges from 330° to 350°, with an inclination of 17° to 23°. From geomorphological point of view, the landslide can be divided into three subzones. The depths of the main slip zone in these subzones from the sliding toe to the head are approximately 61 m (WI1), 46 m (WI2), and 25 m (WI3), respectively (Luo and Huang, 2020). Recent studies have revealed that the upper part of the landslide has replaced the lower one as the most active subzone, which is also revealed by the left side of Fig. 3a. In addition, a shallower secondary slip zone that was newly generated at a depth of about 10 m was identified (Ye et al., 2022). Overall, the deformation of the landslide shows a trend of being less controlled by fluctuations in the RWL as the distance from the river increases and tends to be controlled by rainfall (Yang et al., 2024; Ye et al., 2024d). Initially, it was regarded as a reservoir-induced, seepage-driven retrogressive landslide, particularly in the years following the impoundment. In recent years, however, it has increasingly been considered a rainfall-dominated, seepage-driven compound landslide, characterized by a combination of thrust-type and retrogressive slides.

2.1.2. Xinpu landslide

The younger Xinpu landslide is located downstream of the Outang landslide, on the right bank of the Yangtze River. This landslide affected the entire village, with a total area of 0.86 km^2 and a volume of 5.4 × 10^7 m^3. Notably, this large-scale complex landslide with an unknown mechanism did not receive attention until 2020. For instance, the maximum surface displacement exceeded an astonishing 550 mm from mid-May to early July 2020 (Zhu et al., 2024). There were concerns about possible landslide domino effect inducing landslide, debris flow, surge, or landslide dam and downstream flood. Unlike the Outang landslide, however, there were very limited investigations for this landslide, which compromised our ability to trace the history of the landslide and understand its deformation mechanism.

The elevations of the landslide range from almost 90 to 700 m.a.s.l., with an average slope of 18–28°. The slip zone soils are mainly composed of gray-black or yellow-brown silty clay with a small amount of gravel, gray-black carbonaceous shale interbedded with mudstone. The bedrock attitude is 340°-350°∠21°-26°. Surface velocity vectors show that the lower part of the slide is the most active sector (Fig. 3a), with multiple potential slip surfaces involving local weak layers, the interface between gravelly silty clay and fractured sandstone, and the base-cover interface. The Xinpu landslide currently features shallow sliding, characterized by a mixture of seepage-driven and buoyancy-driven behaviors within the landslide. The magnitude of deformation is correlated with the filling and drawdown of the RWL and rainfall (Zheng et al., 2023a, 2023b; Chang et al., 2024; Zhu et al., 2024).

2.2. Field instrumentation

As shown in Fig. 3, 25 global navigation satellite system (GNSS) surface displacement benchmarks have been successively installed within the Outang landslide since December 2010, and 41 GNSS surface displacement benchmarks have been successively installed within the Xinpu landslide since July 2014. These GNSS surface observations provide the most preliminary information for understanding the kinematics of both landslides. Furthermore, based on several field surveys, multiple boreholes within the active sectors were drilled to acquire subsurface multi-physical information. Specifically, these boreholes were equipped with a microelectromechanical system (MEMS)-based in-place inclinometer array (XP1), a fiber Bragg grating (FBG) strain sensing array (XP2) that is composed of 2 FBG strain sensing cables (i.e., each cable involves 8 gratings), and ultra-weak fiber Bragg grating (UWFBG)-based strain sensing cable in the borehole XP3 within the Xinpu landslide, as well as the borehole OT1 within the Outang landslide. It is worth noting that a distributed temperature sensing (DTS) cable was glued to the outer wall of the casing in borehole XP1. An extra temperature sensing cable was directly embedded in borehole XP2.

For shallow soil temperature and moisture measurements, a set of frequency domain reflectometry (FDR) sensors was installed at depths of 20, 40, 80, and 130 cm at the toe of the Xinpu landslide (Figs. 3 and 4). It also consists of a set of time domain reflectometry (TDR) sensors installed near borehole OT1 at depths of 20, 50, 100, and 150 cm, respectively. In addition, we installed a portable soil temperature and moisture sensor (RC-4) 5 cm below the ground surface. The locations for near-surface soil hydrothermal measurements were determined based on surface velocities measured by GNSS markers and field surveys, focusing on areas where landslide deformations were most active. The aforementioned deep boreholes provided additional reference information on soil temperature, moisture, and strain. Depths within approximately 2 m were identified as the most sensitive range for water-heat exchange (Wu et al., 2023; Zhu et al., 2024), and four representative depths were randomly selected. The probes of TDR and FDR were inserted into the undisturbed soil layer on the side wall of the excavated pit or hole, avoiding contact with gravel.

2.3. Methods

In addition to surface displacement measured by GNSS, the data used in this study mainly involve soil temperature and moisture measurements at depths of interest, as well as strain. Table 1 provides detailed information on the monitoring methods and parameters associated with these measurements for clarity.

2.3.1. TDR

TDR technique involves a probe inserted into the soil, which emits high-frequency electromagnetic pulses and measures the time required for the pulse to return thus inferring the soil moisture content. This principle relies on the fact that the pulse velocity varies with the soil dielectric constant, which increases with increasing moisture content. By analyzing the return time of the pulse, the volumetric water content of the soil can be calculated, as water significantly alters the soil's dielectric properties (Salve, 1998). This method provides accurate, real-time, and non-destructive soil moisture measurements (Dalton, 1992), maintaining an accuracy of 0.02–0.03 m^3/m^3 across various soil types (i.

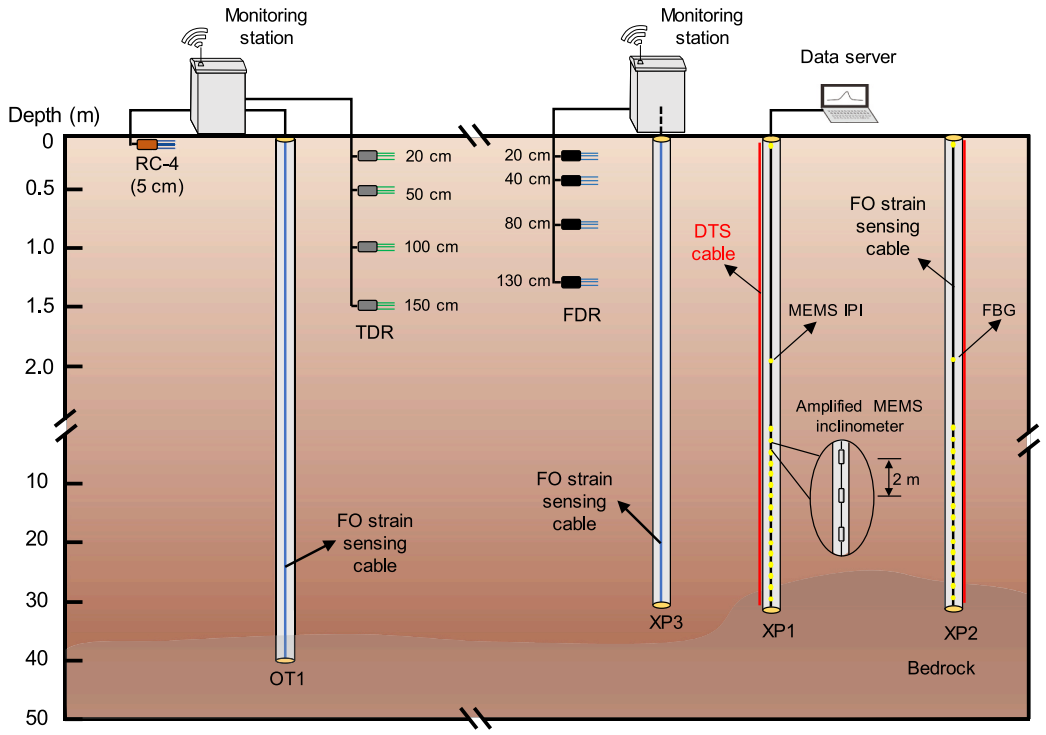

Fig. 4. Illustration of the field deployment of multi-source sensors in the study area.

Table 1
Soil temperature, moisture, and strain measurements and their parametric information.

Methods	Variables measured	Locations	Depths	Accuracy
TDR	Temperature, moisture	around borehole OT1	20, 50, 100, 150 cm	0.5 °C, 0.02 m^3/m^3
RC-4	Temperature, moisture	around borehole OT1	5 cm	–
FDR	Temperature, moisture	around borehole XP2	20, 40, 80, 130 cm	0.5 °C, 0.03 m^3/m^3
UWFBG	Strain	Borehole OT1	Every 1 m	1 με
FBG	Strain	Borehole XP2	Every 2 m	1 με
DTS	Temperature	Boreholes XP1 and XP2	Every 0.2 m	0.2 °C

e., errors within a few percentage points). Moreover, TDR probes are equipped with integrated high-precision temperature sensors, with an accuracy of ±0.5 °C. Consequently, soil temperature can be concurrently measured with soil moisture.

2.3.2. FDR

Similar to TDR, FDR also measures the soil moisture content by analyzing the soil's dielectric constant. The main difference is that TDR measures soil moisture by sending and receiving electromagnetic pulses with time delays, while FDR utilizes changes in the frequency or phase of electromagnetic waves to determine soil moisture (Tran et al., 2015). FDR measurement involves transmitting electromagnetic waves into the soil through a probe (i.e., naturally a capacitance sensor). When the probe is inserted into the soil, an electromagnetic field is generated around the probe. FDR sends continuous electromagnetic waves at one or more frequencies and measures the frequency or phase changes of these waves, thereby obtaining the soil's dielectric constant. As the dielectric constant of water in the soil is much higher than that of dry soil or air, changes in the dielectric constant directly reflect and accurately measure the volumetric water content of the soil, with an accuracy of at least 0.03 m^3/m^3 for typical soils. Similarly, the FDR probe also allows simultaneous measurement of soil temperature together with moisture due to the integrated high-precision temperature sensor with an accuracy of ±0.5 °C.

2.3.3. UWFBG

UWFBG is a special form of FBG with very low reflectivity. The sensing principle of FBG relies on the periodic variation of the refractive index in the optical fiber, which can reflect light of specific wavelengths, known as the Bragg wavelength. Changes in strain or temperature cause variations in the refractive index of the fiber and the grating period, thereby altering the reflected wavelength. By measuring this wavelength shift, FBG can accurately measure strain and temperature.

In an FBG, a large number of weak gratings (i.e., with low reflectivity) is written along a single optical fiber, with each grating independently monitoring strain or temperature (Guo et al., 2024). This configuration limits the signal attenuation at each grating, enabling quasi-distributed monitoring over long distances. UWFBG, interrogated through proper optical schemes (REF), provides a high-sensitivity and wide-range monitoring solution by capturing the changes in reflected wavelength caused by soil strain or temperature variations, with a spatial resolution of 1 m and an accuracy of ±1.0 με/0.1 °C (Ye et al., 2022).

2.3.4. DTS

Distributed temperature sensing (DTS) technology offers an approach for acquiring continuous, high-resolution temperature profiles. This technique typically uses loosely-jacketed optical fibers as sensing elements, leveraging the backscattering phenomena of light signals within the fiber for temperature detection (Fabbian et al., 2024). In essence, DTS interrogator emits a sequence of light pulses through the optical fiber. The majority of these pulses directly propagate along the fiber, whereas a minor fraction undergoes Raman scattering. The intensity of anti-Stokes scattered light is highly sensitive to temperature, exhibiting an increase in intensity with rising temperature. Leveraging Optical Time Domain Reflectometry (OTDR) technology for precise spatial localization, the DTS system calculates the temperature at each

point along the optical fiber by analyzing the intensity ratio of anti-Stokes to Stokes backscattered light. Using the interrogator (NZ-DTS-A01) allows temperature measurement with a spatial resolution of 1 m and an accuracy of 0.1 °C.

2.4. Soil properties

Shallow clayey samples near the two soil moisture stations were collected for particle analysis experiments. As depicted in Fig. 5a, the particle distribution curve indicates that the content of clay particles is approximately 48.2%, silt particles about 44.3%, and sand particles around 7.5%. Fig. 5b shows that the content of clay particles is approximately 43.2%, silt particles about 38.3%, sand particles around 5.7%, and gravel particles 12.8%. According to the soil particle gradation classification in the "Code for investigation of geotechnical engineering" (GB50021–2009), these two geomaterials are classified as silty clay and silty clay with gravel, respectively. Following the "Standard for engineering classification of soil" (GB/T 50145–2007), these soils are identified as well-graded low plasticity clays. The deep soil compositions and structures of the two landslides can be found in Fig. S1.

3. Results and interpretation

3.1. Soil temperature

Fig. 6 provides temperature distributions along two vertical boreholes drilled into the bedrock, with remarkable seasonality. This indicates that the temperature within the sliding mass is strongly influenced by seasonal climate, especially in shallow depths (i.e., within 0–10 m). The soil temperature at the uppermost depth displays the largest fluctuations between winter (e.g., March 17, 2021) and summer (e.g., July 28, 2023). For instance, the temperature on July 28, 2023, reached nearly 40 °C at the surface, as shown in Fig. 6a, while temperatures on March 17, 2021, were below 20 °C. Conversely, all curves tend to stabilize at depths of around 10 m or larger, indicating minimal variations in temperature at these depths regardless of seasons, fluctuating within approximately 18–20 °C. This implies that the temperature variations in shallow soils may be strongly correlated with heat conduction.

Temporally, temperature variations over shorter periods (e.g., several days or months) appear relatively minor, yet significant seasonal patterns are observed from one year to another. These data can be utilized to analyze the thermal stability of landslides and potential seasonal dynamics of water flow, particularly within shallow soils. Given the close distance between these two boreholes, discrepancies in their temperature distributions may suggest variations in the thermal properties of strata and hydrodynamic conditions. Overall, such temperature profiles contribute to a conceptual understanding of the thermodynamics and hydrogeological conditions within the landslide in the reservoir area, which may impact its stability and activity.

Given the emphasis on the sensitive temperature response of shallow soils in Fig. 6, Fig. 7 provides a temperature time series at depths of interest within 1.5 m, alongside air temperature records. Soil temperatures exhibit strong seasonal patterns, with temperature fluctuations decreasing with increasing depth. Peaks are reached during the summer and lows during the winter. The extreme values of soil temperature at shallower depths (e.g., 20 and 50 cm) are more significant compared to those at deeper depths (e.g., cm and 150 cm), showing a wider range of variation (Figs. 7a and S1a). Furthermore, the soil temperature changes at a depth of 5 cm below the surface demonstrate a rapid response to weather events and exhibit fluctuations similar to those of the air temperature (Fig. 7b). Specifically, temperature differences of up to 35 °C were observed at a depth of 5 cm, while temperature variations at a depth of 20 cm also reached approximately 24 °C. The gray dashed lines marking several abrupt air temperature drops indicate that shallow soil exhibits almost no thermal delay, with temperatures quickly following the air temperature. It should be noted that since air temperature drops are often accompanied by precipitation events, soil temperature changes may also reflect seasonal variations in soil moisture, which will be discussed in detail in Section 3.2.

3.2. Soil moisture

Fig. 8 presents the temporal variation in soil moisture content at depths of interest, featuring clear seasonal fluctuations that are closely associated with rainfall events. Across all depths, there is a trend of increased soil moisture content following rainfall events, indicating a rapid infiltration of moisture into these depths, particularly in shallower layers (e.g., within the range of 50 cm). Compared to deeper soils (e.g., 100 and 150 cm), the soil at shallower depths (e.g., 20 and 50 cm) showed more significant fluctuations in water content, in the range of 0.21–0.36 m^3/m^3. This suggests that soil moisture changes at these depths respond more quickly and sensitively to rainfall events, which is partly supported by the measurements from FDR sensors (see

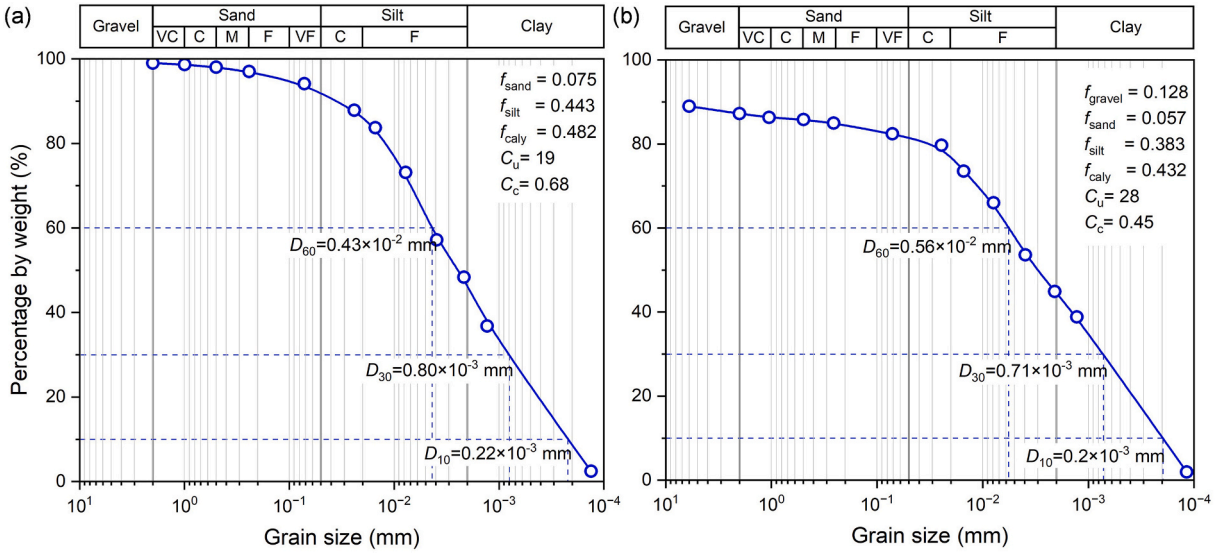

Fig. 5. Grain size distribution curves of representative shallow soils. (a) Silty clay around borehole XP3. (b) Gravelly silty clay around borehole OT1. VC-very coarse; C-coarse; M-medium; F-fine; VF-very fine.

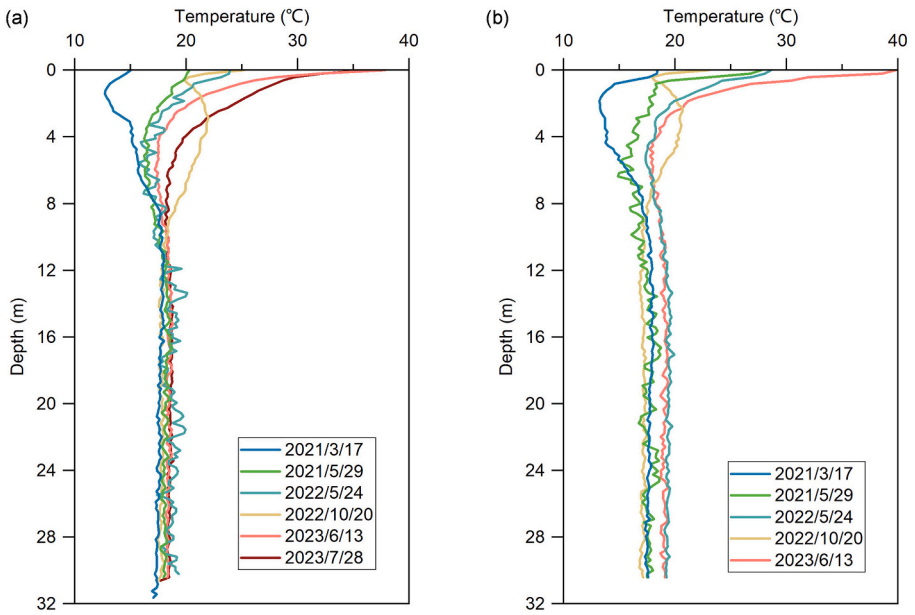

Fig. 6. Borehole-based temperature profiles using distributed temperature sensing (DTS). (a) XP1, FO sensing cable was adhered to the inclinometer case. (b) XP2, FO sensing cable was embedded in the borehole.

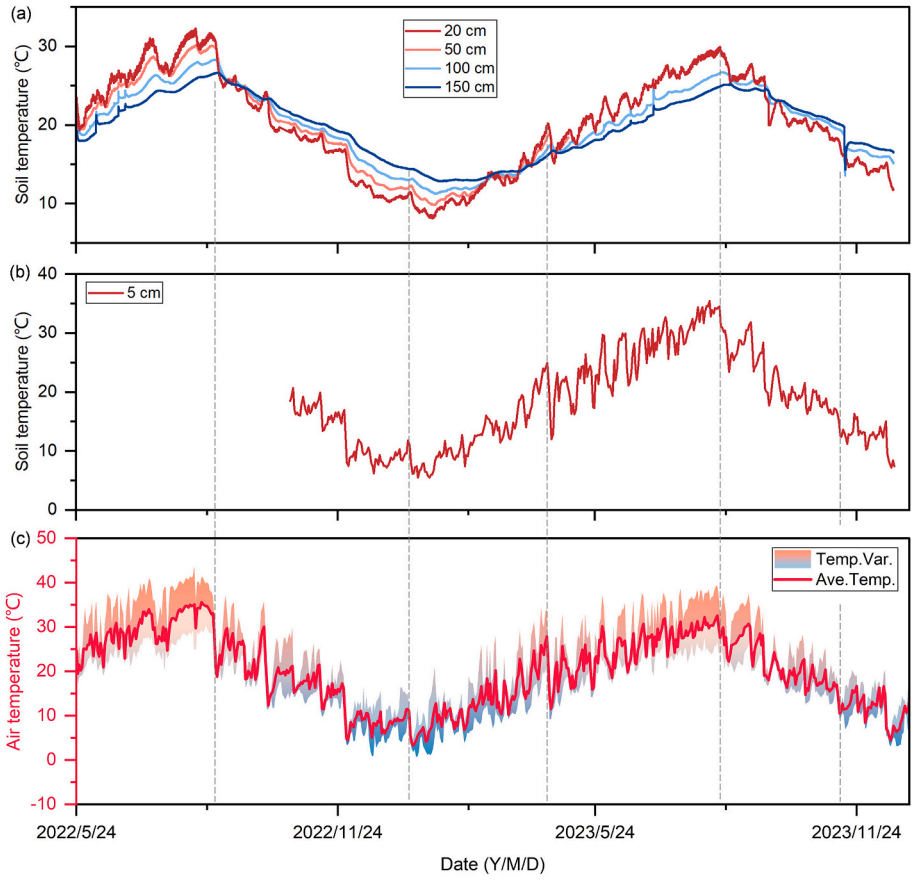

Fig. 7. Temperature observations. (a) Soil temperature using TDR. (b) Soil temperature using RC-4. (c) Air temperature. Dashed lines indicate several abrupt declines in air temperature.

Supplementary Material, Fig. S2b). Conversely, changes in moisture content in deeper soils appeared to respond more prominently to heavy rainfall events or continuous rainfall, mostly ranging from 0.25 to 0.33 m^3/m^3. This is primarily because deeper soils have a stronger capacity of infiltrated rainwater retention, which are less affected by evaporation and plant transpiration. The subsequent decrease in soil moisture content after rainfall events indicates water transport within the soil and/or evaporation. It is noteworthy that the soil moisture content at a depth of

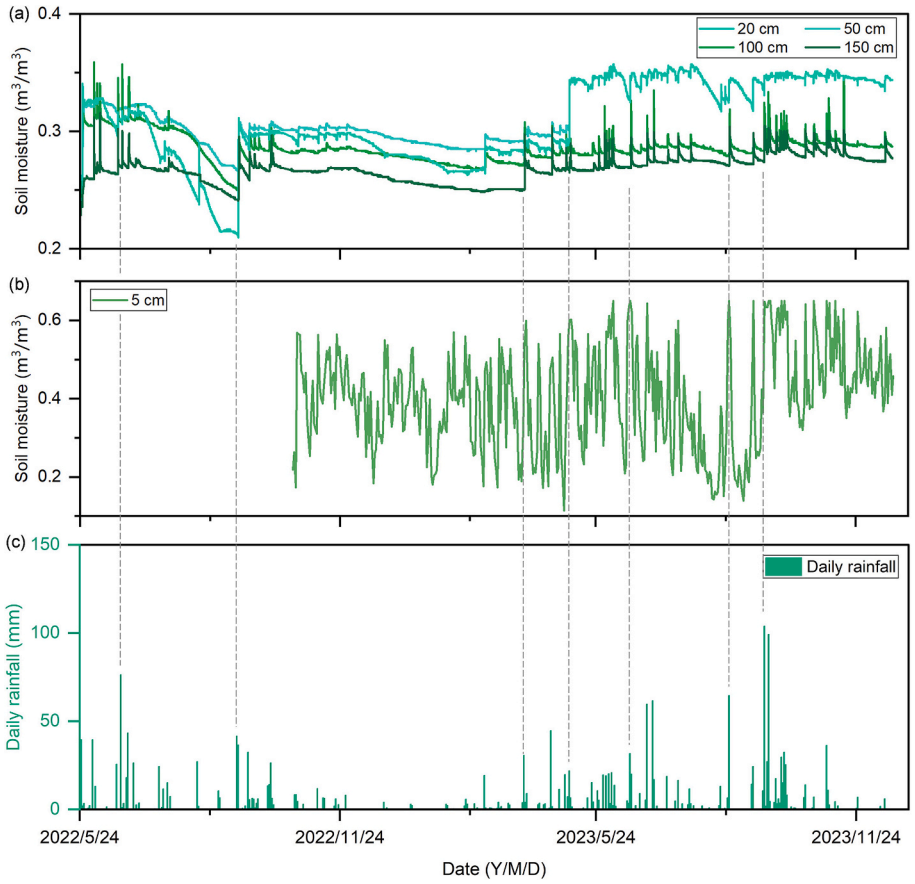

Fig. 8. Moisture observations. (a) Soil moisture using TDR. (b) Soil moisture using RC-4. (c) Rainfall records. A data gap for moisture measurement at a depth of 50 cm is observed, and the reason is unknown.

100 cm is consistently higher than that at 150 cm, despite extremely similar fluctuation patterns. This suggests that the effects of weather events (e.g., high temperature and precipitation) on soil temperature and water content were typically within a depth of 1 m.

As soil moisture conditions themselves reflect past rainfall occurrences, this confirms a positive feedback mechanism between soil moisture and precipitation (Eltahir, 1998). Therefore, these soil moisture contents may serve as near real-time indicators of rainfall events (Ponziani et al., 2023). From a temporal perspective, during the long dry periods in the 2022 monsoon season, it can be observed an overall downward trend of soil moisture contents. This may be attributed to the lack of rainfall replenishment, resulting in enhanced evapotranspiration. Conversely, during the long wet periods in the 2023 monsoon season (i.e., although accompanied by short-term heatwaves), these soil moisture appeared to stabilize, indicating a balance between infiltration and evapotranspiration. Wet soil moisture conditions often enhance net terrestrial radiation by decreasing surface temperatures, increasing atmospheric water vapor content, and increasing downward terrestrial radiation flux simultaneously.

3.3. Landslide deformation

Fig. 9 provides surface and subsurface kinematic behavior for the Xinpu landslide, along with rainfall and RWL records. The GNSS surface displacements closer to the reservoir bank (i.e., G15 and G28) exhibit significant seasonal step-like increases (Fig. 9a), with an annual average rate exceeding 100 mm/yr. Conversely, areas farther from the reservoir bank display insensitive and minor deformation responses (Fig. 9b), largely attributed to the reinforcement effect of the anti-sliding piles AP-4 A' as shown in Fig. 3a. Although these surface records are relatively small but with obvious fluctuations, indicating more of influence from anthropogenic disturbances instead of external hydrometeorological factors. The near-surface strain at a depth of 2 m exhibits considerable fluctuations but no apparent long-term trend (Fig. 9c), possibly reflecting short-term variations in response to external influences such as rainfall. It should be noted that agricultural activities also influenced near-surface strain in that area. Strain at a depth of 4 m is here used to partially represent the kinematics of the shallower slip surface, indicating overall strain accumulation due to shallow shear movements (Fig. 9d). Those slight drawdowns following the accumulation of strain suggest stress release accompanying landslide motions. The strain data at 4 m is used because sensor data from depths between 6 m and 16 m have been unavailable since October 2021, with remarkable strain increase and macroscopic deformation signs. The most probable reason for this data loss, despite the allowable range of the strain measurements, is that angular gravel mixed into the slip zone soils at a depth of around 7 m mechanically damaged the sensor. Strain near the base-cover interface at a depth of 28 m remains relatively stable throughout the observation period, indicating minimal influence from rainfall and RWL changes on this potential deep-seated slip surface (Fig. 9e).

Previous studies and drilling boreholes have successfully identified critical geo-interfaces, such as shallow slip surfaces at depths of ~7 and ~ 12 m, and the bedrock-cover interface at a depth of 28 m (Zhu et al., 2024). The slip surface at a depth of 12 m was not involved in this study because the landslide experienced significant shear movement during the 2021 monsoon season, leading to the failure of the FBG sensors within depths of 6–16 m (Fig. S3a). Rainfall records, particularly for those heavy or continuous rainfall events, may be associated with short-term variations in surface movement and shallow subsurface strain (Kogure and Okuda, 2018; Zhang and Pei, 2024). Additionally,

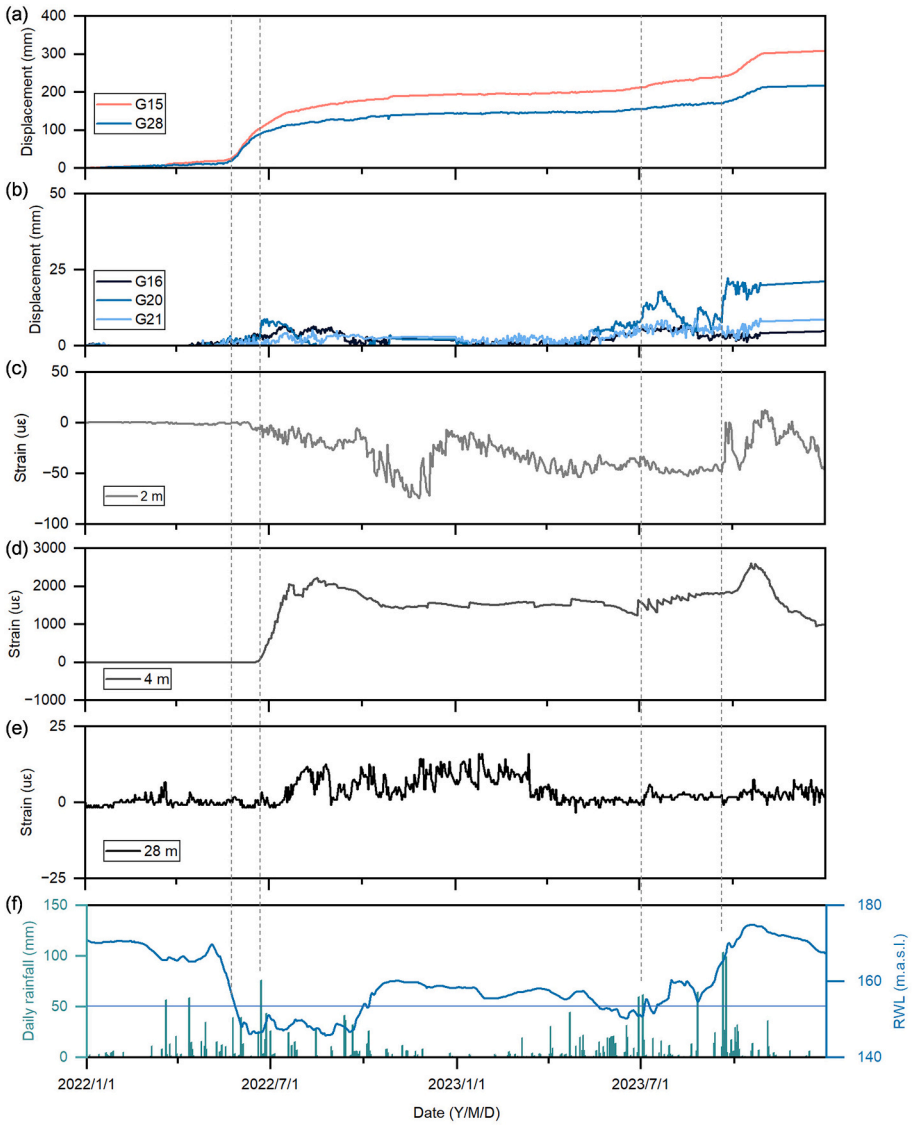

Fig. 9. Surface and subsurface deformation time series of the Xinpu landslide. (a) and (b) GNSS displacement. (c-e) FO strain of near-surface, slip surface, and inactive cover-base interface in borehole XP2. (f) RWL and rainfall records.

continuous RWL rise (i.e., from late August to mid-October 2023) may also have contributed to increases of landslide displacement and strain, making it evolve in a style of buoyancy-driven deformation (Tang et al., 2019; Zhu et al., 2024).

Similarly, Fig. 10 presents surface and subsurface kinematics of the Outang landslide, along with rainfall and RWL records. Our earlier study has identified two potential slip surfaces located at depths of approximately 10 and 20 m (Ye et al., 2022). It can be observed that the landslide deformation appears to be considerably associated with hydrological extremes during the period. In the dry year of 2022, GNSS benchmarks mostly showed very limited displacements, except for L1 closer to the reservoir bank (Fig. 10a). In contrast, the whole landslide featured strong deformation in the wet year of 2023, especially for the upper part of the landslide. Specifically, the displacement increases at L3, M4, and R1 reached almost 90, 46, and 180 mm, respectively, which were 1.7–5.5 times those in the previous year. Consistent with surface displacements, the strain curves at three depths of interest suggest that rainfall plays a primary controlling role in landslide deformation (Figs. 10b-10d). For instance, the rainfall event on June 22, 2022 (i.e., daily rainfall reached 76.4 mm), significantly triggered strain accumulation reaching the slip surface at 10 m depth but did not extend to deeper slip surfaces. Negative strain values indicate compression at the optical cable. Likewise, consecutive heavy rainfall events on September 20 (i.e., 103.9 mm) and September 23, 2023 (i.e., 99.3 mm), activated remarkable deep-seated slip, characterized by sharp increases in strain. At this time, the optical cable was under tension due to the shearing action of sliding masses. The response of strains at both slip surfaces was also supported by the GNSS measurements, consistently demonstrating the controlling effect of rainfall on the whole landslide kinematics (Ye et al., 2024b). However, apart from the influence of rainfall, the increase in displacement near the shore (i.e., L1) during the monsoon season in 2022 might be driven by the lowering of RWL (Luo and Huang, 2020).

3.4. Correlation between landslide deformation and hydrometeorological factors

Soil temperature and moisture measurements from TDR are used as part of critical hydrometeorological factors for analysis, due to the substantial data gaps in FDR measurements during the monitoring period (Fig. S2b). Nonetheless, FDR measurements partially provide some reference for evaluating and interpreting the TDR measurements. Landslide deformations are characterized by surface displacements and

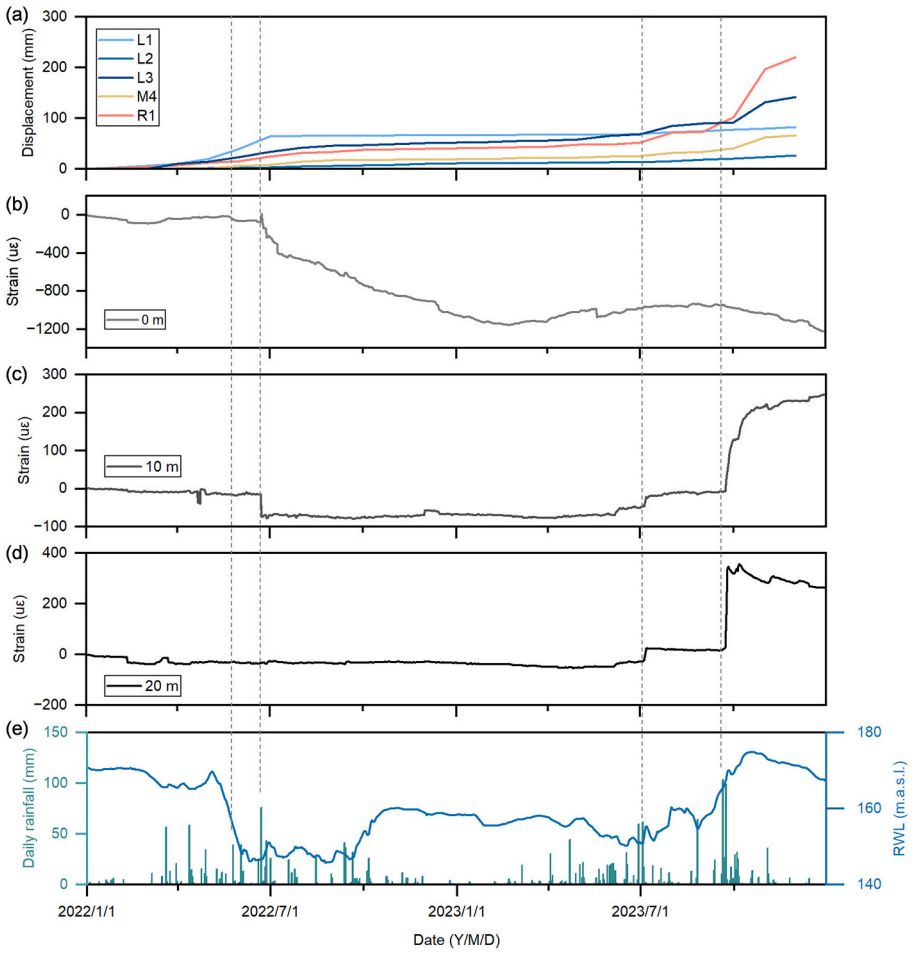

Fig. 10. Surface and subsurface deformation time series of the Outang landslide. (a) GNSS displacement. (b-d) FO strain of near-surface, slip surfaces at depths of almost 10 and 20 m in borehole OT1. (e) RWL and rainfall records.

strains at depths of interest, for instance, strain at depths of 2 m, 4 m, 28 m for the Xinpu landslide in borehole XP2, and at depths of 0 m, 10 m, 20 m for the Outang landslide in borehole OT1. Although these sensors were deployed in two different landslides, their spatial proximity and similar deployment settings in terms of topographical and geotechnical conditions allow for the exploration of correlations between respective landslide activities and shared data on soil temperature and moisture. Fig. 11 provides the Pearson correlation coefficient (PCC) matrices of

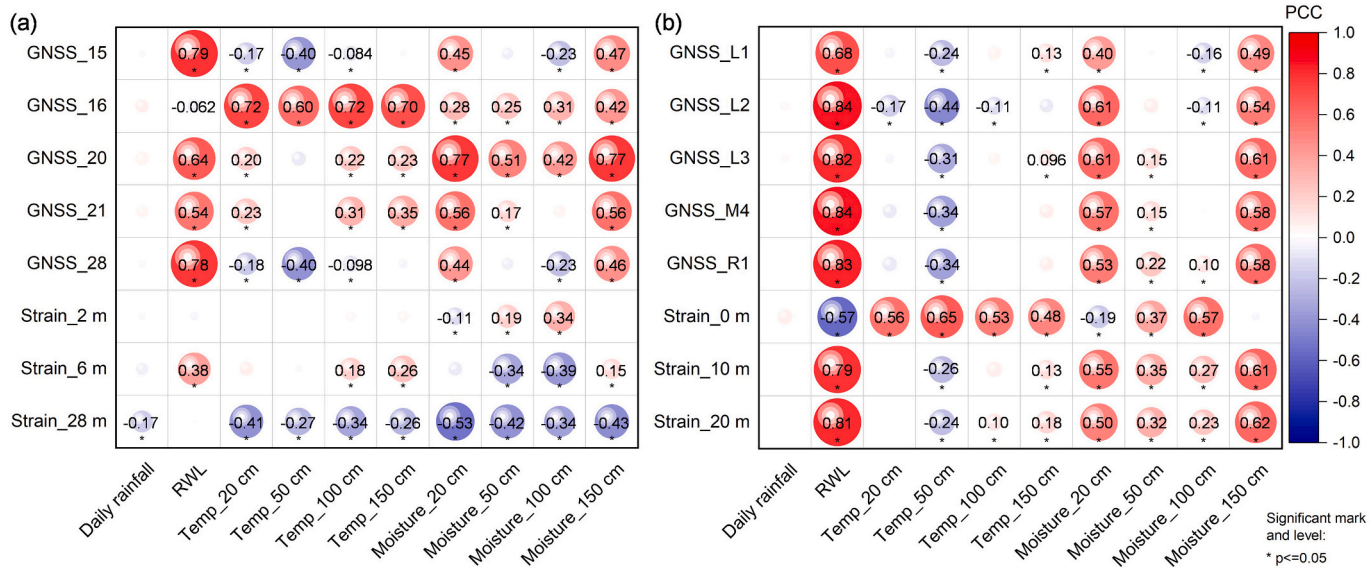

Fig. 11. Correlation map between landslide deformations and soil temperatures and moistures. (a) Xinpu landslide. (b) Outang landslide.

two landslide monitoring datasets, illustrating the relationships between landslide deformations and hydro-climatically environmental factors. The values of the correlation coefficient range from −1 to 1, with values close to 1 or − 1 indicating strong correlation, positive values indicating positive correlation, and vice versa. The color and size of the circles represent the strength of the correlation, and values marked with asterisks indicate statistical significance ($p \leq 0.05$).

In Fig. 11a, GNSS benchmarks G15 and G28 exhibit a strong positive correlation with RWL (PCC reaching 0.79), indicating a significant influence of RWL rise on the displacements of these two points (i.e., the lower part of the landslide close to the reservoir bank). GNSS benchmarks G16, G20, and G21 show moderate to strong positive correlations with soil temperature/moisture (e.g., 20 and 50 cm depths) (PCC ranging from 0.51 to 0.77), which may suggest a close relationship between soil temperature and moisture content changes, also implying their triangular relationship with the displacements. Here strains at near-surface and base-cover interface are not further analyzed due to considerable human disturbances or limited changes during the monitoring period. The strain near the slip surface (at a depth of 6 m) shows a moderate positive correlation with RWL (PCC of 0.38), indicating the control of RWL rise on this shallow landslide movement. Additionally, it exhibits moderate negative correlations with soil moisture at depths of 50 and 100 cm (PCC of −0.34 and − 0.39, respectively), but positive correlations with soil temperature at depths of 100 and 150 cm, which typically indicates intense soil evaporation and little rainfall, pointing to a scenario of RWL rise at the end of the monsoon season (i.e., normally from late August to early September). Overall, multifaceted analyses confirm the control of RWL rise on this landslide kinematic behavior, in a style of shallow movement. This is consistent with the buoyancy-driven deformation mechanism reported in previous studies (Zhu et al., 2024).

In Fig. 11b, it appears that all GNSS displacements and FO strains show strong positive correlations with RWL (PCC ranging from 0.68 to 0.84). However, this does not mean that the filling of RWL is the primary control of landslide deformation. On the contrary, continuous and/or heavy rainfall is the dominant triggering factor for the entire landslide. This is because most of the landslide deformation occurred during the overlapping periods of consecutive heavy rainfall events and RWL rise (i.e., on September 20 and 23, 2023, in Fig. 10e), resulting in artifacts related to statistics. On the other hand, these measurements show moderate to strong correlations with soil moisture at a depth of 20 cm (PCCs ranging from 0.4 to 0.61), while showing moderate negative correlations with soil temperatures at a depth of 50 cm (PCCs around −0.3), implying remarkable infiltration effects in rainy scenarios. In particular, the strong positive correlation with soil moisture at a depth of 150 cm reflects the contribution of intense rainfall with greater infiltration depth.

Together, the changes in near-surface soil temperature and moisture content (especially at depths of 20 and 50 cm) exhibit certain correlations with changes in surface displacements and slip surface strains. These relationships are significant for understanding the mechanisms and drivers of landslides, as well as developing predictive models for landslide risk alerts. On the other hand, the data attributes of daily rainfall, which often involve non-uniformly distributed extreme values, place high demands on most time series prediction models. This results in a significant underestimation of direct assessments of landslide activity when correlated with rainfall data (see the first column in Fig. 11). Along with soil temperature, in-situ soil moisture data effectively contain useful information about the hydrological and geomechanical evolution in shallow soils and even down to deep-seated slip surfaces during extreme rainfall events (Ye et al., 2022, 2024d). In particular, the seasonal variation of shallow soil temperature and moisture content help to distinguish time windows of specific hydrological events. This allows us to potentially differentiate the main controlling factors of landslide deformation, even in compound scenarios overlapping rainfall events and RWL fluctuations, based on certain prior knowledge of landslide kinematics or mechanisms (Yin et al., 2016; Luo and Huang, 2020; Ye et al., 2024b).

4. Discussion

4.1. Influence of extreme weather events on landslide activity

Previous studies have highlighted the overwhelming impact of extreme weather events on landslide activity, especially extreme intense rainfall (Ye et al., 2022, 2024b). To further understand the temporal patterns of these extreme events, we investigated the annual distribution characteristics at a decadal timescale in the study area and identified thresholds of extremely high temperature and rainfall events (Text S1; Figs. S4 and S5). Fig. 12 shows the occurrence of extreme weather during 2012–2023. It is worth noting that 72.7% of extreme high temperature events occurred in August, while extreme rainfall events mainly occurred in June, July, August, and September, accounting for 22.7%, 22.7%, 15.9%, and 18.2%, respectively. These findings support the fact that landslide deformation primarily occurs during these months, even though additional influences such as RWL fluctuations and human activity may also be involved. Another crucial point to highlight is that concurrent extreme weather conditions are becoming increasingly common (Araújo et al., 2022; Ozturk et al., 2022; Stevenson et al., 2022), implying that extreme droughts often coincide with intra-annual or inter-annual extreme rainfall events (Tichavský et al., 2019; Handwerger et al., 2019; De Luca et al., 2020; Guo et al., 2023a; Ye et al., 2024d). These intensified weather extremes are highly likely to impact and be feedback on the variations in shallow soil temperature and moisture. Therefore, real-time measurements of depth-of-interest soil temperature and moisture at the hillslope scale are expected to help establish a more promising risk warning framework.

4.2. Broader implications for landslide monitoring, forecasting, and early warning

Soil moisture is considered a critical factor in the feedback mechanisms influencing weather patterns and precipitation (Eltahir, 1998). Apart from reflecting direct responses to rainfall events as an alternative precipitation indicator, changes and retention of soil moisture in deeper soils also reflect the transport of pore fluids in porous media and their interaction with the atmosphere (Ye et al., 2022). Changes in volumetric moisture content can also be linked to soil moisture saturation. When large and interconnected areas of a hillslope become saturated (i.e., high volumetric moisture content and low standard deviation of water saturation), additional water cannot redistribute to empty drier areas and potentially increase local pore water pressures and seepage force, leading to intensified shear deformation and failure (Lehmann et al., 2013; Schenato et al., 2017). Particularly, terraces of unique topography in this region may amplify the local hydromechanical effect during heavy/continuous rainfall scenarios (Ye et al., 2022). Recent studies have shown improved landslide prediction performance with the inclusion of soil hydrological information. This demonstrates the potential of in-situ soil moisture measurements for landslide warning, both at regional and hillslope scales (Wicki et al., 2020; Distefano et al., 2023). Soil temperature is typically not a direct triggering factor but still plays an important role in hydrological analysis. These temperature and moisture measurements with distinct seasonal characteristics are expected to be linked to the multi-annual kinematics of reservoir landslides, making it possible to forecast landslide displacements and decipher potential triggering factors of deformation using interpretable deep learning models (Loche and Scaringi, 2024; Ma et al., 2024).

4.3. Limitations and further considerations of the study

This study provides an in-situ monitoring dataset of shallow soil temperature and moisture content at depths of interest within an active

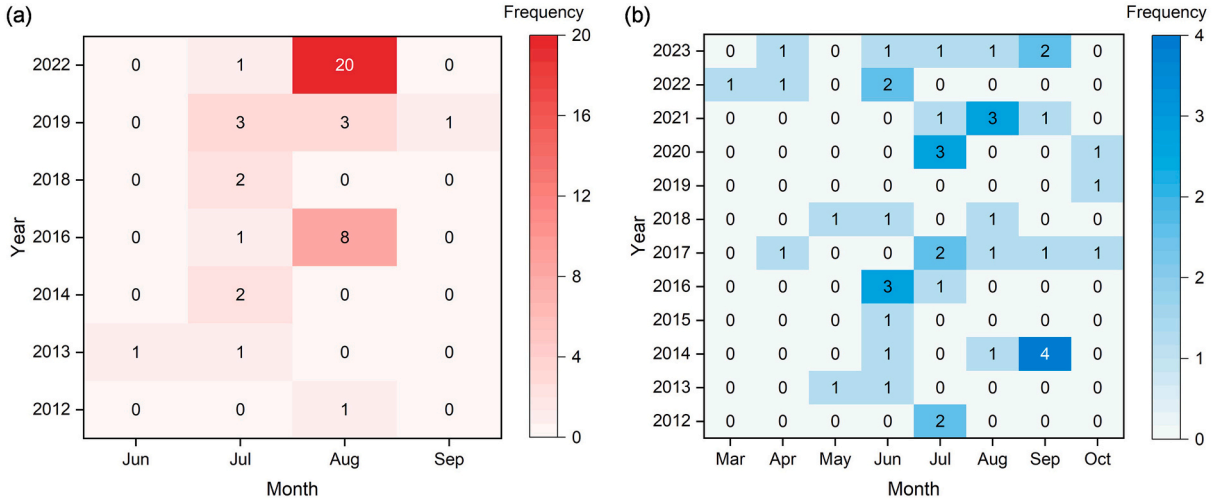

Fig. 12. Annual and seasonal distribution of extreme weather events during 2012–2023. (a) Extreme high temperature. (b) Extreme rainfall.

landslide subzone, to investigate the correlation between landslide activity and these parameters. Despite the gathered data covering two complete monsoon seasons, representing two typical hydrological extremes, longer-term data coverage and/or more hydro-related measurements are advocated. Beyond that, these two landslide cases presented in this study feature north-facing terrains. Future considerations will involve distinguishing the orientation and vegetation factors of landslides to investigate their effects on shallow soil temperature and moisture content, as well as landslide activity (McGuire et al., 2016; Xiang et al., 2023). The absence of vegetation can exacerbate these soil temperature differences, thereby affecting soil moisture and evapotranspiration, and eventually influencing the rainfall threshold for triggering mass movements. On the other hand, due to the rainfall recharge, there is a close hydraulic connection between landslide groundwater and the Yangtze River water. Therefore, another consideration for future research is to explore the differences in chemical ion concentrations in soil water and their migration, revealing the complex hydromechanical interaction between rainfall and sliding masses (Dai et al., 2015).

5. Conclusions

This paper presents a crucial dataset of soil temperature and moisture data at specific depths that were collected using multiple sensors (FDR, TDR, FO, and RC-4) in real time. The aim was to investigate the correlation between landslide activity and soil temperature and moisture by analyzing the kinematic behavior of a pair of neighboring slow-moving landslides. Field monitoring provided the firsthand data, allowing insights into the vertical distribution and responding characteristics of shallow soil temperature and moisture under different hydrometeorological conditions. Pearson correlation analysis was employed to examine the relationship between landslide deformation and environmental variables. For the Xinpu landslide, the landslide activity was strongly positively correlated with RWL, indicating that RWL rise tends to trigger landslide deformation. Meanwhile, it exhibited a moderate negative correlation with soil moisture content (e.g., at depths of 20 and 150 cm) and a weak positive correlation with soil temperature (e.g., at a depth of 50 cm), suggesting slight rainfall infiltration and strong soil evaporation. This essentially points to the controlling effect of RWL rise on the landslide movement. Conversely, for the Outang landslide, the landslide activity showed a moderate to strong correlation with soil moisture (i.e., at a depth of 20 cm) and a moderate negative correlation with soil temperature (i.e., at a depth of 50 cm), indicating significant rainfall infiltration effect in the rainy season. This essentially indicates rainfall control over landslide movement, especially during heavy continuous rainfall. Overall, variations in near-surface soil temperatures and moistures within a depth of 150 cm provide feedback on landslide dynamics and deformation mechanisms. This demonstrates the significance of in-situ monitoring and field surveys, and suggests that the engineering geological analogy method should be approached with caution, as the landslides, although geographically close, are likely to exhibit distinct kinematic behaviors and triggering mechanisms. It is worth noting that the daily rainfall data attributes may lead to statistical artifacts in Pearson correlation. Along with soil temperature, in-situ soil moisture data effectively contain valuable information on the evolution of shallow soils and even deep-seated slip surfaces in response to hydrometeorological events.

This work highlights the importance of multi-source, multi-physical monitoring in revealing the complex interaction mechanisms of landslides, particularly noting the overlooked role of near-surface thermo- and hydro-related measurements in landslide activity. The identification of 44 extreme high temperature events and 44 extreme rainfall events occurring in the study area over the past twelve years, suggests that surface temperature and moisture may contribute to probing feedback mechanisms between extreme events and soil thermo-hydrological behavior under climate warming conditions, challenging the traditional view that temperature is insignificant in landslide monitoring. Standing on the shoulder of these two slow-moving landslide cases, we call for the urgency to better understand these natural phenomena under climate warming conditions.

CRediT authorship contribution statement

Xiao Ye: Writing – original draft, Software, Methodology, Investigation, Data curation, Conceptualization. **Hong-Hu Zhu:** Writing – review & editing, Supervision, Resources, Project administration, Funding acquisition, Conceptualization. **Bing Wu:** Visualization, Software, Formal analysis. **Feng Tian:** Software, Investigation, Data curation. **Wei Zhang:** Writing – review & editing, Investigation. **Xie Hu:** Writing – review & editing, Conceptualization. **Luca Schenato:** Writing – review & editing, Methodology. **Alessandro Pasuto:** Writing – review & editing, Funding acquisition, Formal analysis. **Filippo Catani:** Writing – review & editing, Conceptualization.

Declaration of competing interest

The authors declare that they have no known competing financial interests or personal relationships that could have appeared to influence the work reported in this paper.

Data availability

Data will be made available on request.

Acknowledgments

This work was funded by the of National Natural Science Foundation of China [Grant agreement No. 42225702], and supported from the Maria Skłodowska-Curie Action - UPGRADE (mUltiscale IoT equipPed lonG linear infRastructure resilience built and sustAinable DevelopmEnt) project - HORIZON-MSCA-2022-SE-01 [101131146] and the project "The Geosciences for Sustainable Development" [CUP C93C23002690001] of Department of Geosciences, University of Padova. The first author particularly acknowledges the China Scholarship Council (CSC) for funding his research period at UNIPD and CNR-IRPI. The authors wish to express their gratitude to Jing Wang, Tiancheng Xie, Jie Li, and Ning Ma at NJU for their assistance in field instrumentation. Additionally, special thanks are extended to Assoc. Prof. Mario Floris, Assoc. Prof. Ascanio Rosi at UNIPD, and Dr. Giulia Bossi at CNR-IRPI for their insightful comments and suggestions on our manuscript.

Appendix A. Supplementary data

Supplementary data to this article can be found online at https://doi.org/10.1016/j.enggeo.2024.107690.

References

Ahmad, S.M., Sadhasivam, N., Lisa, M., Lombardo, L., Emil, M.K., Zaki, A., Van Westen, C.J., Fadel, I., Tanyas, H., 2024. Standing on the shoulder of a giant landslide: a six-year long InSAR look at a slow-moving hillslope in the western Karakoram. Geomorphology 444, 108959. https://doi.org/10.1016/j.geomorph.2023.108959.

Alonso, E.E., Zervos, A., Pinyol, N.M., 2016. Thermo-poro-mechanical analysis of landslides: from creeping behaviour to catastrophic failure. Géotechnique 66 (3), 202–219. https://doi.org/10.1680/jgeot.15.LM.006.

Araújo, J.R., Ramos, A.M., Soares, P.M.M., Melo, R., Oliveira, S.C., Trigo, R.M., 2022. Impact of extreme rainfall events on landslide activity in Portugal under climate change scenarios. Landslides 19, 2279–2293. https://doi.org/10.1007/s10346-022-01895-7.

Chang, Z.L., Huang, F.M., Huang, J.S., Jiang, S.H., Liu, Y.T., Meena, S.R., Catani, F., 2023. An updating of landslide susceptibility prediction from the perspective of space and time. Geosci. Front. 14 (5), 101619 https://doi.org/10.1016/j.gsf.2023.101619.

Chang, F.N., Dong, S.C., Yin, H.W., Ye, X., Zhang, W., Zhu, H.H., 2024. Temporal stacking of sub-pixel offset tracking for monitoring slow-moving landslides in vegetated terrain. Landslides 21, 1255–1271. https://doi.org/10.1007/s10346-024-02227-7.

Dai, Z.W., Yin, Y.P., Wei, Y.J., Lv, T., Luo, J.H., Yao, W., 2015. Characteristics, origin and formation mechanism of the Outang landslide in the three Gorges Reservoir area. Hydrogeology & Engineering Geology 42 (6), 145–153. https://doi.org/10.16030/j.cnki.issn.1000-3665.2015.06.23.

Dalton, F.N., 1992. Development of time-domain reflectometry for measuring soil water content and bulk soil electrical conductivity. Advances in measurement of soil physical properties: Bringing theory into practice 30, 143–167. https://doi.org/10.2136/sssaspecpub30.c8.

De Luca, P., Messori, G., Wilby, R.L., Mazzoleni, M., Di Baldassarre, G., 2020. Concurrent wet and dry hydrological extremes at the global scale. Earth Syst. Dynam. 11, 251–266. https://doi.org/10.5194/esd-11-251-2020.

Distefano, P., Peres, D.J., Piciullo, L., Palazzolo, N., Scandura, P., Cancelliere, A., 2023. Hydro-meteorological landslide triggering thresholds based on artificial neural networks using observed precipitation and ERA5-Land soil moisture. Landslides 20, 2725–2739. https://doi.org/10.1007/s10346-023-02132-5.

Eltahir, E.A.B., 1998. A soil moisture-rainfall feedback mechanism: 1. Theory and observations. Water Resour. Res. 34 (4), 765–776. https://doi.org/10.1029/97WR03499.

Fabbian, N., Simonini, P., De Polo, F., Schenato, L., Cola, S., 2024. Temperature monitoring in levees for detection of seepage. Bull. Eng. Geol. Environ. 83, 69. https://doi.org/10.1007/s10064-024-03566-4.

Fang, K., Miao, M.H., Tang, H.M., Jia, S.X., Dong, A., An, P.J., Zhang, B.C., 2023. Insights into the deformation and failure characteristic of a slope due to excavation through multi-field monitoring: a model test. Acta Geotech. 18, 1001–1024. https://doi.org/10.1007/s11440-022-01627-0.

Fang, K., Dong, A., Tang, H.M., An, P.J., Wang, Q.Y., Jia, S.X., Zhang, B.C., 2024. Development of an easy-assembly and low-cost multismartphone photogrammetric monitoring system for rock slope hazards. Int. J. Rock Mech. Min. Sci. 174, 105655 https://doi.org/10.1016/j.ijrmms.2024.105655.

Froude, M.J., Petley, D., 2018. Global fatal landslide occurrence from 2004 to 2016. Nat. Hazards Earth Syst. Sci. 18, 2161–2181. https://doi.org/10.5194/nhess-18-2161-2018.

Goren, L., Aharonov, E., 2007. Long runout landslides: the role of frictional heating and hydraulic diffusivity. Geophys. Res. Lett. 34 (7), L07301. https://doi.org/10.1029/2006GL028895.

Goren, L., Aharonov, E., 2009. On the stability of landslides: a thermo-poro-elastic approach. Earth Planet. Sci. Lett. 277 (3–4), 365–372. https://doi.org/10.1016/j.epsl.2008.11.002.

Guo, J.H., Wang, X.Q., Fan, Y.R., Liang, X., Jia, H.T., Liu, L.L., 2023a. How extreme events in China would be affected by global warming-Insights from a bias-corrected CMIP6 ensemble. *Earth's*. Future 11. https://doi.org/10.1029/2022EF003347 e2022EF003347.

Guo, J.Y., Shi, B., Sun, M.Y., Zhang, C.C., Tang, C.S., Wei, G.Q., Fang, J.H., Jiang, H.T., 2023b. Soil total suction sensing using fiber-optic technology. Geoderma 439, 116687. https://doi.org/10.1016/j.geoderma.2023.116687.

Guo, J.Y., Fang, J.H., Shi, B., Zhang, C.C., Liu, L., 2024. High-sensitivity water leakage detection and localization in tunnels using novel ultra-weak fiber Bragg grating sensing technology. Tunn. Undergr. Sp. Tech. 144, 105574 https://doi.org/10.1016/j.tust.2023.105574.

Han, Q.Q., Zeng, Y.J., Zhang, L.J., Cira, C.I., Prikaziuk, E., Duan, T., Wang, C., Szabó, B., Manfreda, S., Zhuang, R.D., Su, B., 2023. Ensemble of optimised machine learning algorithms for predicting surface soil moisture content at a global scale. Geosci. Model Dev. 16 (20), 5825–5845. https://doi.org/10.5194/gmd-16-5825-2023.

Handwerger, A.L., Huang, M.H., Fielding, E.J., Booth, A.M., Bürgmann, R., 2019. A shift from drought to extreme rainfall drives a stable landslide to catastrophic failure. Sci. Rep. 9, 1569. https://doi.org/10.1038/s41598-018-38300-0.

He, S.M., Liu, W., Wang, J., 2015. Dynamic simulation of landslide based on thermo-poro-elastic approach. Comput. Geosci. 75, 24–32. https://doi.org/10.1016/j.cageo.2014.10.013.

Hu, X., Bürgmann, R., Schulz, W.H., Fielding, E.J., 2020. Four-dimensional surface motions of the Slumgullion landslide and quantification of hydrometeorological forcing. Nat. Commun. 11, 2792. https://doi.org/10.1038/s41467-020-16617-7.

Kirschbaum, D., Kapnick, S.B., Stanley, T., Pascale, S., 2020. Changes in extreme precipitation and landslides over High Mountain Asia. Geophys. Res. Lett. 47 https://doi.org/10.1029/2019GL085347 e2019GL085347.

Kogure, T., Okuda, Y., 2018. Monitoring the vertical distribution of rainfall-induced strain changes in a landslide measured by distributed fiber optic sensing with Rayleigh backscattering. Geophys. Res. Lett. 45, 4033–4040. https://doi.org/10.1029/2018GL077607.

Lacroix, P., Handwerger, A.L., Bièvre, G., 2020. Life and death of slow-moving landslides. Nat. Rev. Earth Environ. 1 (8), 404–419. https://doi.org/10.1038/s43017-020-0072-8.

Lehmann, P., Gambazzi, F., Suski, B., Baron, L., Askarinejad, A., Springman, S.M., Holliger, K., Or, D., 2013. Evolution of soil wetting patterns preceding a hydrologically induced landslide inferred from electrical resistivity survey and point measurements of volumetric water content and pore water pressure. Water Resour. Res. 49 (12), 7992–8004. https://doi.org/10.1002/2013WR014560.

Liu, Y.T., Teza, G., Nava, L., Chang, Z.L., Shang, M., Xiong, D.B., Cola, S., 2024. Deformation evaluation and displacement forecasting of baishuihe landslide after stabilization based on continuous wavelet transform and deep learning. Nat. Hazards. https://doi.org/10.1007/s11069-024-06580-7.

Loche, M., Scaringi, G., 2023. Temperature and shear-rate effects in two pure clays: possible implications for clay landslides. Results Eng. 20, 101647 https://doi.org/10.1016/j.rineng.2023.101647.

Loche, M., Scaringi, G., 2024. Assessing the influence of temperature on slope stability in a temperate climate: A nationwide spatial probability analysis in Italy. https://doi.org/10.31223/X5Z09H.

Loche, M., Scaringi, G., Yunus, A.P., Catani, F., Tanyaş, H., Frodella, W., Fan, X., Lombardo, L., 2022. Surface temperature controls the pattern of post-earthquake landslide activity. Sci. Rep. 12, 988. https://doi.org/10.1038/s41598-022-04992-8.

Luo, S.L., Huang, D., 2020. Deformation characteristics and reactivation mechanisms of the Outang ancient landslide in the three Gorges Reservoir. Chin. Bull. Eng. Geol. Environ. 79, 3943–3958. https://doi.org/10.1007/s10064-020-01838-3.

Ma, Z.J., Mei, G., 2024. Forecasting landslide deformation by integrating domain knowledge into interpretable deep learning considering spatiotemporal correlations. J. Rock Mech. Geotech. Eng. https://doi.org/10.1016/j.jrmge.2024.02.034.

Ma, Z.J., Mei, G., Xu, N.X., 2024. Characterizing seasonality and trend from in situ time-series observations using explainable deep learning for ground deformation forecasting. J. Geophys. Res. Mach. Learn. Comput. 1 https://doi.org/10.1029/2024JH000122 e2024JH000122.

Martelloni, G., Segoni, S., Lagomarsino, D., Fanti, R., Catani, F., 2013. Snow accumulation/melting model (SAMM) for integrated use in regional scale landslide early warning systems. Hydrol. Earth Syst. Sci. 17, 1229–1240. https://doi.org/10.5194/hess-17-1229-2013.

McGuire, L.A., Rengers, F.K., Kean, J.W., Coe, J.A., Mirus, B.B., Baum, R.L., Godt, J.W., 2016. Elucidating the role of vegetation in the initiation of rainfall-induced shallow landslides: Insights from an extreme rainfall event in the Colorado Front Range. Geophys. Res. Lett. 43, 9084–9092. https://doi.org/10.1002/2016GL070741.

Nava, L., Carraro, E., Reyes-Carmona, C., Puliero, S., Bhuyan, K., Rosi, A., Monserrat, O., Floris, M., Meena, S.R., Galve, J.P., Catani, F., 2023. Landslide displacement forecasting using deep learning and monitoring data across selected sites. Landslides 20, 2111–2129. https://doi.org/10.1007/s10346-023-02104-9.

Ng, C.W.W., Zhang, Q., Zhou, C., Ni, J.J., 2022. Eco-geotechnics for human sustainability. Sci. China Tech. Sci. 65, 2809–2845. https://doi.org/10.1007/s11431-022-2174-9.
Ozturk, U., Bozzolan, E., Holcombe, E.A., Shukla, R., Pianosi, F., Wagener, T., 2022. How climate change and unplanned urban sprawl bring more landslides. Nature 608, 262–265. https://doi.org/10.1038/d41586-022-02141-9.
Patton, A.I., Rathburn, S.L., Capps, D.M., McGrath, D., Brown, R.A., 2021. Ongoing landslide deformation in thawing permafrost. Geophys. Res. Lett. 48 https://doi.org/10.1029/2021GL092959 e2021GL092959.
Pei, H.F., Zhang, F., Zhu, H.H., Liu, J.M., Ning, F.W., Chen, W., 2023. Development of a distributed three-dimensional inclinometer based on OFDR technology and the Frenet-Serret equations. Measurement 223, 113769. https://doi.org/10.1016/j.measurement.2023.113769.
Pinyol, N.M., Alonso, E.E., 2010. Criteria for rapid sliding II.: thermo-hydro-mechanical and scale effects in Vaiont case. Eng. Geol. 114 (3–4), 211–227. https://doi.org/10.1016/j.enggeo.2010.04.017.
Pinyol, N.M., Alvarado, M., Alonso, E.E., Zabala, F., 2018. Thermal effects in landslide mobility. Géotechnique 68 (6), 528–545. https://doi.org/10.1680/jgeot.17.P.054.
Ponziani, F., Ciuffi, P., Bayer, B., Berni, N., Franceschini, S., Simoni, A., 2023. Regional-scale InSAR investigation and landslide early warning thresholds in Umbria, Italy. Eng. Geol. 327, 107352 https://doi.org/10.1016/j.enggeo.2023.107352.
Salve, R., 1998. Near-surface wetting of a ponded basalt surface: observations using time domain reflectometry. J. Hydrol. 208 (3–4), 249–261. https://doi.org/10.1016/S0022-1694(98)00167-X.
Schenato, L., Palmieri, L., Camporese, M., Bersan, S., Cola, S., Pasuto, A., Galtarossa, A., Salandin, P., Simonini, P., 2017. Distributed optical fibre sensing for early detection of shallow landslides triggering. Sci. Rep. 7, 14686. https://doi.org/10.1038/s41598-017-12610-1.
Seguí, C., Veveakis, M., 2021. Continuous assessment of landslides by measuring their basal temperature. Landslides 18, 3953–3961. https://doi.org/10.1007/s10346-021-01762-x.
Shi, X., Hu, X., Sitar, N., Kayen, R., Qi, S., Jiang, H., Wang, X., Zhang, L., 2021. Hydrological control shift from river level to rainfall in the reactivated Guobu slope besides the Laxiwa hydropower station in China. Remote Sens. Environ. 265, 112664 https://doi.org/10.1016/j.rse.2021.112664.
Shibasaki, T., Matsuura, S., Okamoto, T., 2016. Experimental evidence for shallow, slow-moving landslides activated by a decrease in ground temperature. Geophys. Res. Lett. 43, 6975–6984. https://doi.org/10.1002/2016GL069604.
Stevenson, S., Coats, S., Touma, D., Cole, J., Lehner, F., Fasullo, J., Otto-Bliesner, B., 2022. Twenty-first century hydroclimate: a continually changing baseline, with more frequent extremes. Proc. Natl. Acad. Sci. U. S. A. 119 (12), e2108124119 https://doi.org/10.1073/pnas.2108124119.
Sun, M.Y., Shi, B., Zhang, C.C., Zheng, X., Guo, J.Y., Wang, Y.Q., He, M.N., Liu, J., 2021. Quasi-distributed fiber-optic in-situ monitoring technology for large-scale measurement of soil water content and its application. Eng. Geol. 294, 106373 https://doi.org/10.1016/j.enggeo.2021.106373.
Sun, M.Y., Shi, B., Zhang, C.C., Liu, J., Guo, J.Y., Zheng, X., Wang, Y.Q., Wei, G.Q., 2022. Quantifying the spatio-temporal variability of total water content in seasonally frozen soil using actively heated fiber Bragg grating sensing. J. Hydrol. 606, 127386 https://doi.org/10.1016/j.jhydrol.2021.127386.
Tang, H.M., Wasowski, J., Juang, C.H., 2019. Geohazards in the three Gorges Reservoir area, China-Lessons learned from decades of research. Eng. Geol. 261, 105267 https://doi.org/10.1016/j.enggeo.2019.105267.
Tichavský, R., Ballesteros-Cánovas, J.A., Šilhán, K., Tolasz, R., Stoffel, M., 2019. Dry spells and extreme precipitation are the main trigger of landslides in Central Europe. Sci. Rep. 9, 14560. https://doi.org/10.1038/s41598-019-51148-2.
Tran, A.P., Bogaert, P., Wiaux, F., Vanclooster, M., Lambot, S., 2015. High-resolution space–time quantification of soil moisture along a hillslope using joint analysis of ground penetrating radar and frequency domain reflectometry data. J. Hydrol. 523, 252–261. https://doi.org/10.1016/j.jhydrol.2015.01.065.
Veveakis, E., Vardoulakis, I., Di Toro, G., 2007. Thermoporomechanics of creeping landslides: the 1963 Vaiont slide, northern Italy. Case Rep. Med. 112 (F3), F03026. https://doi.org/10.1029/2006JF000702.
Voight, B., Faust, C., 1982. Frictional heat and strength loss in some rapid landslides. Géotechnique 32 (1), 43–54. https://doi.org/10.1680/geot.1982.32.1.43.
Wang, J., Lin, S.Q., Tan, D.Y., Yin, J.H., Zhu, H.H., Kuok, S.C., 2024. A novel method for integrity assessment of soil-nailing works with actively heated fiber-optic sensors. J. Geotech. Geoenviron. Eng. 150 (8), 04024063. https://doi.org/10.1061/JGGEFK.GTENG-11790.
Wicki, A., Lehmann, P., Hauck, C., Seneviratne, S.I., Waldner, P., Stähli, M., 2020. Assessing the potential of soil moisture measurements for regional landslide early warning. Landslides 17, 1881–1896. https://doi.org/10.1007/s10346-020-01400-y.
Wistuba, M., Gorczyca, E., Malik, I., Yu, R.D., Ślęzak, A., 2024. Divergent patterns of landslide activity and triggering factors at a local scale of a single mountain massif (Island Beskid Mts., Western Carpathians, Poland). Eng. Geol. 335, 107531 https://doi.org/10.1016/j.enggeo.2024.107531.
Wu, B., Zhu, H.H., Cao, D.F., Xu, L., Shi, B., 2021. Feasibility study on ice content measurement of frozen soil using actively heated FBG sensors. Cold Reg. Sci. Technol. 39, 103332 https://doi.org/10.1016/j.coldregions.2021.103332.
Wu, B., Zhu, H.H., Cao, D.F., Liu, X.F., Liu, T.X., 2023. Fiber optic sensing-based field investigation of thermo-hydraulic behaviors of loess for characterizing land-atmosphere interactions. Eng. Geol. 315, 107019 https://doi.org/10.1016/j.enggeo.2023.107019.
Xiang, Z.L., Dou, J., Yunus, A.P., Zhang, L.L., Wang, X.K., Luo, W.Q., 2023. Vegetation-landslide nexus and topographic changes post the 2004 Mw 6.6 Chuetsu earthquake. Catena 223, 106946. https://doi.org/10.1016/j.catena.2023.106946.
Xie, T.C., Zhu, H.H., Tan, D.Y., Shukla, S.K., 2024. Modeling pipe-soil interaction under surface loading using material point method. Tunn. Undergr. Sp. Tech. 147, 105709 https://doi.org/10.1016/j.tust.2024.105709.
Yang, B.B., Liu, Z.Q., Lacasse, S., Liang, X., 2024. Spatiotemporal deformation characteristics of Outang landslide and identification of triggering factors using data mining. J. Rock Mech. Geotech. Eng. https://doi.org/10.1016/j.jrmge.2023.09.030.
Ye, X., Zhu, H.H., Wang, J., Zhang, Q., Shi, B., Schenato, L., Pasuto, A., 2022. Subsurface multi-physical monitoring of a reservoir landslide with the fiber-optic nerve system. Geophys. Res. Lett. 49 (11) https://doi.org/10.1029/2022GL098211 e2022GL098211.
Ye, B.F., Qiu, H.J., Tang, B.Z., Liu, Y., Liu, Z.J., Jiang, X.Y., Yang, D.D., Ullah, M., Zhu, Y. R., Kamp, U., 2024a. Creep deformation monitoring of landslides in a reservoir area. J. Hydrol. 632, 130905 https://doi.org/10.1016/j.jhydrol.2024.130905.
Ye, X., Zhu, H.H., Chang, F.N., Xie, T.C., Tian, F., Zhang, W., Catani, F., 2024b. Revisiting spatiotemporal evolution process and mechanism of a giant reservoir landslide during weather extremes. Eng. Geol. 332, 107480 https://doi.org/10.1016/j.enggeo.2024.107480.
Ye, X., Zhu, H.H., Cheng, G., Pei, H.F., Shi, B., Schenato, L., Pasuto, A., 2024c. Thermo-hydro-poro-mechanical responses of a reservoir-induced landslide tracked by high-resolution fiber optic sensing nerves. J. Rock Mech. Geotech. Eng. 16 (3), 1018–1032. https://doi.org/10.1016/j.jrmge.2023.04.004.
Ye, X., Zhu, H.H., Wang, J., Zheng, W.J., Zhang, W., Schenato, L., Pasuto, A., Catani, F., 2024d. Towards hydrometeorological thresholds of reservoir-induced landslide from subsurface strain observations. Sci. China Technol. Sci. 67 (6), 1907–1922. https://doi.org/10.1007/s11431-023-2657-3.
Yin, Y.P., Huang, B.L., Wang, W.P., Wei, Y.J., Ma, X.H., Ma, F., Zhao, C., 2016. Reservoir-induced landslides and risk control in three Gorges Project on Yangtze River, China. J. Rock Mech. Geotech. Eng. 8, 577–595. https://doi.org/10.1016/j.jrmge.2016.08.001.
Zeng, T.R., Yin, K.L., Jiang, H.W., Liu, X.P., Guo, Z.Z., Peduto, D., 2022. Groundwater level prediction based on a combined intelligence method for the Sifangbei landslide in the three Gorges Reservoir Area. Sci. Rep. 12, 11108. https://doi.org/10.1038/s41598-022-14037-9.
Zeng, T.R., Glade, T., Xie, Y.Y., Yin, K.L., Peduto, D., 2023. Deep learning powered long-term warning systems for reservoir landslides. Int. J. Disast. Risk Re. 94, 103820 https://doi.org/10.1016/j.ijdrr.2023.103820.
Zeng, T., Gong, Q.B., Wu, L.Y., Zhu, Y.H., Yin, K.L., Peduto, D., 2024a. Double-index rainfall warning and probabilistic physically based model for fast-moving landslide hazard analysis in subtropical-typhoon area. Landslides 21, 753–773. https://doi.org/10.1007/s10346-023-02187-4.
Zeng, T., Wu, L.Y., Hayakawa, Y.S., Yin, K.L., Gui, L., Jin, B.J., Guo, Z.Z., Peduto, D., 2024b. Advanced integration of ensemble learning and MT-InSAR for enhanced slow-moving landslide susceptibility zoning. Eng. Geol. 331, 107436 https://doi.org/10.1016/j.enggeo.2024.107436.
Zhang, F., Pei, H.F., 2024. Stability analysis of shallow slopes under rainfall infiltration considering tensile strength cut-off. Comput. Geotech. 171, 106327 https://doi.org/10.1016/j.compgeo.2024.106327.
Zheng, W.J., Hu, J., Lu, Z., Hu, X., Sun, Q., Liu, J.H., Zhu, J.J., Li, Z.W., 2023a. Enhanced kinematic inversion of 3-D displacements, geometry, and hydraulic properties of a North-south slow-moving landslide in three Gorges Reservoir. J. Geophys. Res. Solid Earth 128 (6). https://doi.org/10.1029/2022JB026232 e2022JB026232.
Zheng, W.J., Sun, Q., Hu, J., Lu, Z., Zhu, K., Ye, X., Huang, G.W., Hu, M.J., Zhu, J.J., Li, Z.W., 2023b. Investigating kinematics and triggers of slow-moving reservoir landslide using an improved MT-InSAR method. Geomat. Nat. Haz. Risk 14 (1), 2289835. https://doi.org/10.1080/19475705.2023.2289835.
Zhou, C., Cao, Y., Yin, K.L., Intrieri, E., Catani, F., Wu, L.X., 2022. Characteristic comparison of seepage-driven and buoyancy-driven landslides in three Gorges Reservoir area. China. Eng. Geol. 301, 106590 https://doi.org/10.1016/j.enggeo.2022.106590.
Zhou, C., Cao, Y., Gan, L.L., Wang, Y., Motagh, M., Roessner, S., Hu, X., Yin, K.L., 2024. A novel framework for landslide displacement prediction using MT-InSAR and machine learning techniques. Eng. Geol. 334, 107497 https://doi.org/10.1016/j.enggeo.2024.107497.
Zhu, H.H., 2023. Engineering geological interface: from multivariate characterization to evolution mechanism. Bull. Geol. Sci. Technol. 42 (1), 1–20. https://doi.org/10.19509/j.cnki.dzkq.tb20220661 (in Chinese).
Zhu, H.H., Wu, B., Cao, D.F., Li, B., Wen, Z., Liu, X.F., Shi, B., 2023. Characterizing thermo-hydraulic behaviors of seasonally frozen loess via a combined opto-electronic sensing system: Field monitoring and assessment. J. Hydrol. 622, 129647 https://doi.org/10.1016/j.jhydrol.2023.129647.
Zhu, H.H., Ye, X., Pei, H.F., Zhang, W., Cheng, G., Li, Z.L., 2024. Probing multi-physical process and deformation mechanism of a large-scale landslide using integrated dual-source monitoring. Geosci. Front. 15 (2), 101773 https://doi.org/10.1016/j.gsf.2023.101773.